15 GHz VLA OBSERVATIONS OF THE RADIO GALAXIES 3C 166 AND 3C 411

ALAN L. FEY, STEVEN R. SPANGLER, AND STEVEN T. MYERS
Department of Physics and Astronomy, The University of Iowa, Iowa City, Iowa 52242
Received 17 December 1985; revised 4 March 1986

ABSTRACT

We present 15 GHz Very Large Array observations of the luminous double radio galaxies 3C 166 and 3C 411. Our data confirm the spectral steepening in the lobes of both sources indicated by previous lower-frequency observations. The spectral steepening is interpreted as being due to synchrotron-radiation losses (synchrotron aging) and is used to infer a radiative age for electrons in both lobes of 3C 411 and the southern lobe of 3C 166. We present the results as a relative speed of separation between the hot spot and a parcel of lobe material. The speed estimates, in the range of one to a few times 10^4 km/s, are comparable to values determined for other radio sources. Our observations also suggest that for both sources geometric depolarization is responsible for the reduction in fractional linear polarization at frequencies of 5 GHz and above.

I. INTRODUCTION

The NRAO* Very Large Array (VLA) is an excellent instrument for studying the low-surface-brightness lobe or bridge emission observed in radio galaxies. In scaled array mode, multifrequency, high-dynamic-range maps with similar (u, v) plane coverage and resolution can be made. In this paper we present 15 GHz VLA observations of the radio galaxies 3C 166 and 3C 411. These observations, together with previous scaled-array VLA observations at 1.4 and 5 GHz, are used to study the frequency dependence of total intensity and polarization characteristics across these sources. Previous observations at 1.4 and 5 GHz have been reported by Spangler and Bridle (1982) for 3C 166 and Spangler and Pogge (1984) for 3C 411.

The previous lower-frequency observations indicated some common features of 3C 166 and 3C 411. First, both sources show pronounced spectral steepening in one or both lobes, with the spectral index steepening with distance from the hot spot. The spectral data were analyzed by Myers and Spangler (1985), and used to obtain estimates for the relative speed of separation of the hot spots and lobe material. Second, in parts of both sources, depolarization is observed, i.e., a lower value for the fractional linear polarization at 1.4 GHz than at 5 GHz. Depolarization indicates the presence of Faraday rotation, either in the radio-emitting material or in an external plasma. Furthermore, the observed 5 GHz fractional linear polarization is observed to be considerably below the theoretical maximum value. On the basis of 1.4 and 5 GHz observations, one cannot exclude the possibility that Faraday depolarization could be important at 5 GHz.

The 15 GHz observations reported in this paper were undertaken to answer some of the questions raised by the earlier observations. Since synchrotron-radiation losses are more pronounced at 15 than at 5 GHz, 2 cm observations provide the opportunity to confirm the identification of radiative losses, and refine quantitative results, such as radiative lifetimes. Faraday-rotation effects are also substantially smaller at 15 GHz, allowing one to distinguish between Faraday and geometric mechanisms for reducing the degree of linear polarization.

*The National Radio Astronomy Observatory is operated by Associated Universities, Inc., under contract from the National Science Foundation.

II. OBSERVATIONS AND DATA REDUCTION

Observations at 15 GHz were made with the Very Large Array on 28–29 April 1984. Both sources were observed over an approximately 12 hr interval, with on-source observing times of about 6 hr and 4 hr for 3C 411 and 3C 166, respectively. Observations were made in two 50 MHz *IF* bandpasses, one centered at 14964.9 MHz, and the other at 14914.9 MHz. Amplitude and initial phase calibration was accomplished by frequent observations of the sources 0735 + 178 and 2029 + 121, which served as calibrators for 3C 166 and 3C 411, respectively. The derived 15 GHz flux densities of these sources were 0.658 ± 0.003 Jy for 2029 + 121 and 1.97 ± 0.01 Jy for 0735 + 178. The quoted uncertainties are formal ones, resulting from scatter in the measurements on different baselines. These sources were also used for determination of the instrumental polarization. The absolute polarization position angle was determined by observations of 3C 286 and 3C 138.

Following standard external calibration, the data were submitted to self-calibration. This task was facilitated in the cases of 3C 166 and 3C 411 by the prominence of the source central components. Antenna gains were determined on baselines that were sufficiently long to resolve out the extended emission, leaving only the point-like central components.

Data from the two *IF* channels were independently calibrated, mapped, and cleaned. Maps of the Stokes parameters *I*, *Q*, and *U* from the two channels were then summed after inspection to ensure that no anomalies, such as position offsets, preferentially affected data from one *IF*. The mapping and subsequent image analysis were carried out using the NRAO Astronomical Image Processing System (AIPS).

One of the goals of the present observations was to study the frequency dependence of total intensity across the extended lobes in these sources (see Sec. IV below). A study of this nature requires that the multifrequency maps have the same effective resolution. To this end, the 15 GHz maps were processed in a manner identical to the 1.4 and 5 GHz maps. The restoring beams have diameters (FWHM) of 1.6 arcsec for 3C 166 and 1.5 arcsec for 3C 411. The 3C 411 images presented below have been rotated -23 deg with respect to their orientation on the sky.

A discussion of the acquisition, calibration, and mapping of the 1.4 and 5 GHz data is given in Spangler and Bridle

 0004-6256/86/061279-07$00.90

(1982) for 3C 166 and in Spangler and Pogge (1984) for 3C 411.

III. OBSERVATIONAL RESULTS

a) Spectral Characteristics

Maps of 3C 166 and 3C 411 at 1.4 and 15 GHz are shown in Figs. 1 and 2, respectively. These figures illustrate the regions of primary interest, namely the extended lobe or radio bridge emission thought to be produced by energetic electrons that were initially accelerated in the hot spots. Inspection of the total intensity maps indicates that the lobes in both sources are rather weak at 15 GHz compared to 1.4 GHz. We now discuss each source in detail.

1) 3C 166

We have restricted our analysis to the southern lobe of 3C 166. It is more luminous than the northern lobe and has a bright rim and hot spot at its outer edge. Figure 3 shows the map observables on a slice along the source axis. Figure 3(a) shows the 1.4 GHz total intensity, while Figs. 3(b) and 3(c) show the 1.4–5 and 5–15 GHz spectral index data, respectively. The curves represent models for synchrotron-radiation losses, which are described in Sec. IV below. It is evident from Fig. 3 that both the 1.4–5 and 5–15 GHz spectral indices remain roughly constant upon leaving the hot spot and then steepen with distance from the hot spot. The conversion from angular to linear size has been made using an image scale of 2.5 kpc/arcsec. The redshift of 3C 166 is 0.246.

2) 3C 411

The data for the Sf and Np lobes of 3C 411 are shown in Figs. 4 and 5. Again the slices have been taken along the source axis. Assuming a Hubble constant of 100 km/s/Mpc, a redshift of $z = 0.469$ for this object gives an image scale of 3.4 kpc/arcsec.

Figure 4(a) shows the 1.4 GHz total intensity along the source axis for the Sf lobe. The 1.4–5 and 5–15 GHz spectral-index data for the Sf lobe are shown in Figs. 4(b) and 4(c), respectively. The 1.4–5 GHz spectral index is seen to steepen rapidly upon leaving the hot spot and then remain relatively constant across the rest of the lobe. The 5–15 GHz spectral index, on the other hand, steepens monotonically with distance from the hot spot. In the case of this lobe, the 5–15 GHz spectral index is observed to be less than -2.

The spectral steepening on the leading edge of the hot spot is believed to be artifactual, arising from very slight offsets in the maps at different frequencies. The measured spectral index is highly susceptible to such effects in regions of large intensity gradients. To test this explanation, spectral-index curves such as those shown in Fig. 4 were calculated with a range of small but plausible offsets between the maps at the two frequencies. It was found that offsets of even a tenth of an arcsecond were sufficient to change the spectral index in the regions of large intensity gradients. Depending on the choice of offset, the spectral-index curve through the hot spot could be flattened, or even made to harden on the leading edge. We emphasize that such adjustments have no discernible effect on spectral index measurements in the lobes, which are the regions of importance to our analysis. We have

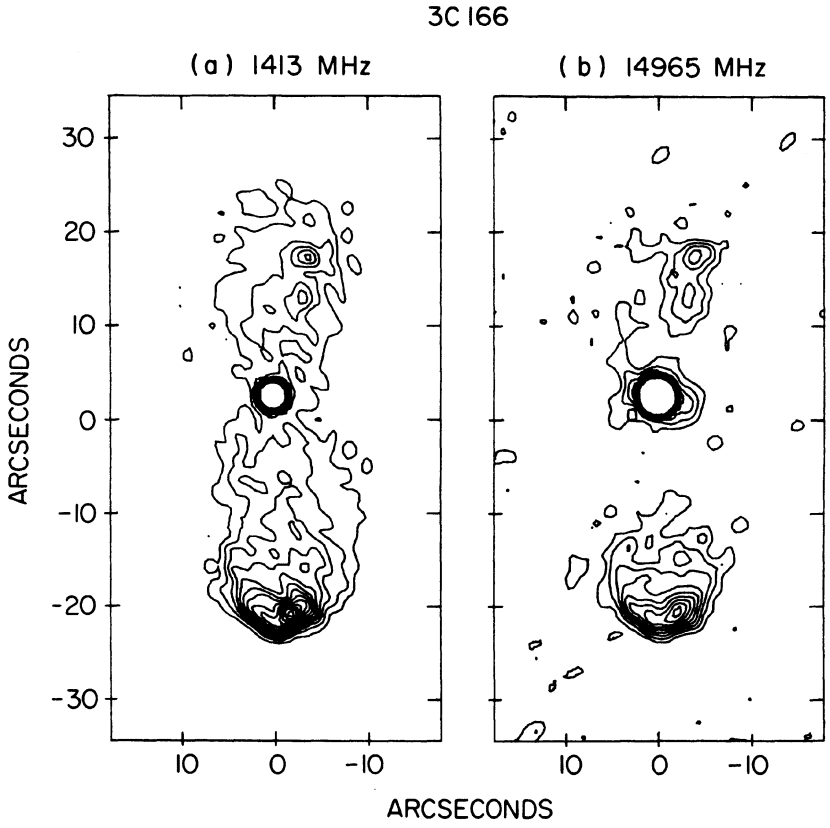

FIG. 1. Total intensity maps of 3C 166. (a) At 1.413 GHz; there are 15 evenly spaced contours beginning at 1% of the peak intensity, which is 0.369 Jy/beam. (b) At 14.965 GHz; contours are the same as in (a) but begin at 0.15% of the peak intensity, which is 0.386 Jy/beam. The restoring beam is 1.6 arcsec (FWHM) for both maps.

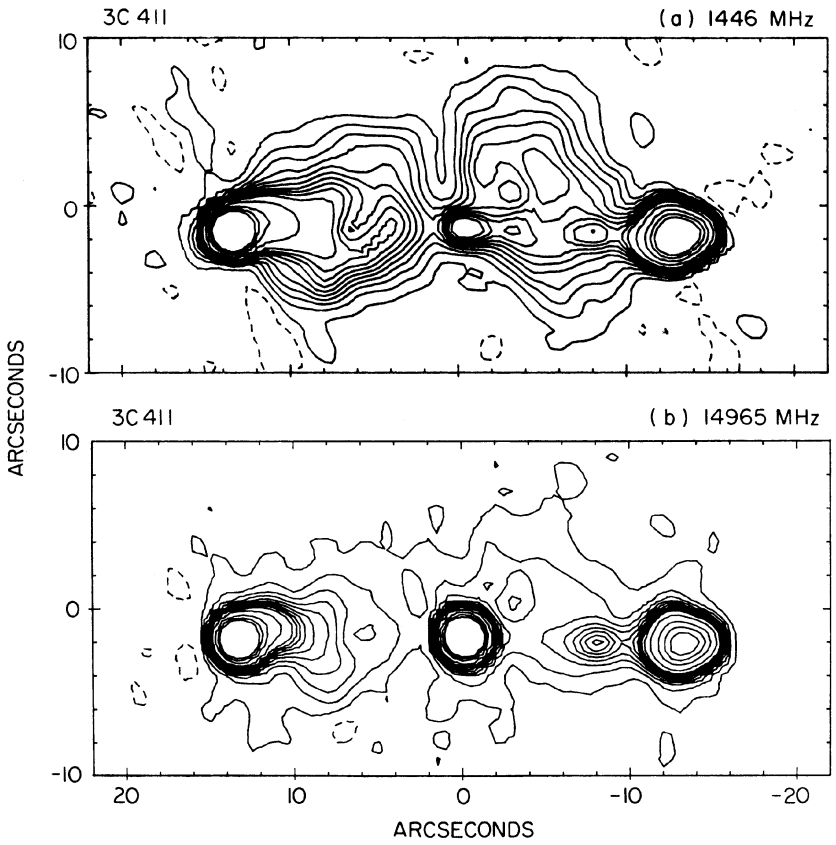

FIG. 2. Total intensity maps of 3C 411 at 1.446 GHz (a) and 14.965 GHz (b). Contours are at −0.25 (dashed contour), 0.25, 0.75, 1.25, 1.75, 2.25, 2.75, 3.25, 3.75, 4.25, 5, 7.5, 12.5, 17.5, and 22.5% of the peak intensity, which is 0.657 Jy/beam at 1.446 GHz and 0.091 Jy/beam at 14.965 GHz. The restoring beam is 1.5 arcsec (FWHM) for both maps.

therefore chosen to retain the independently determined positioning of the maps, cognizant of the strong possibility that spectral-index errors of order 0.1 may be present in regions of steep intensity gradients.

Figure 5(a) shows the 1.4 GHz total intensity along the source axis for the Np lobe. The 1.4–5 and 5–15 GHz spectral-index slices for the Np lobe are shown in Figs. 5(b) and 5(c), respectively. Because of the possible presence of a jet in this lobe, the interpretation of the spectral-index gradient is less straightforward. The possible jet, located between the hot spot and central component, is seen to have a relatively flat spectrum, as expected (Bridle 1982).

b) Central Components

1) 3C 166

The central component of 3C 166 has a flat spectrum, typical of compact extragalactic radio sources. The flux density at 15 GHz is 383 ± 4 mJy/beam. At 1.4 and 5 GHz the flux density is 361 ± 3 and 435 ± 2 mJy/beam, respectively. The frequency of flux-density maximum is therefore in the vicinity of 5 GHz. The fractional linear polarization of the central component is 2.0 ± 0.1% at 15 GHz. This represents an increase in fractional linear polarization over a value of 1.1 ± 0.1% at both 1.4 and 5 GHz.

We note that the sky coordinates of the central component are R.A.(1950) = $6^h42^m24^s.67$, Dec.(1950) = 21°25′2″.4.

2) 3C 411

The flux density of the central component at 15 GHz is 91 ± 1 mJy/beam. This represents an increase over the values of 45 ± 2 mJy/beam at 5 GHz and 28 ± 2 mJy/beam at 1.4 GHz, thus confirming that the spectrum of the central component is inverted (Spangler and Pogge 1984). The fractional linear polarization at 15 GHz is less than 1%, as is the case at 1.4 and 5 GHz. Polarized emission near the center of the source appears to be significantly displaced from the central component (as may be seen in Fig. 6), a characteristic that is again consistent with the presence of a jet. The coordinates of the central component are R.A.(1950) = $20^h19^m44^s.20$, Dec.(1950) = 9°51′33″.4.

c) Polarization Characteristics

1) 3C 166

Significant polarized emission was detected only from the forward "ridge" in the southern lobe and the central component. Elsewhere the surface brightness of the emission was too low to permit worthwhile polarimetric measurements. The polarized emission that is seen in the southern lobe confirms the report in Spangler and Bridle (1982) that the inferred magnetic field is circumferential at the lobe periphery.

At 1.4 and 5 GHz, the interior of the southern lobe is weakly polarized, with higher fractional polarization at 5 than at 1.4 GHz (Spangler and Bridle 1982). One of the purposes of the present observations was to determine if geometric or Faraday depolarization was responsible for the reduction from the theoretical maximum of the 5 GHz fractional polarization. Near the leading edge of the lobe the 15 GHz fractional polarization is of order 5–10%, comparable to the values observed at 5 GHz and much larger than those at 1.4 GHz. This suggests geometric depolarization at frequencies of 5 GHz and above for this portion of the source.

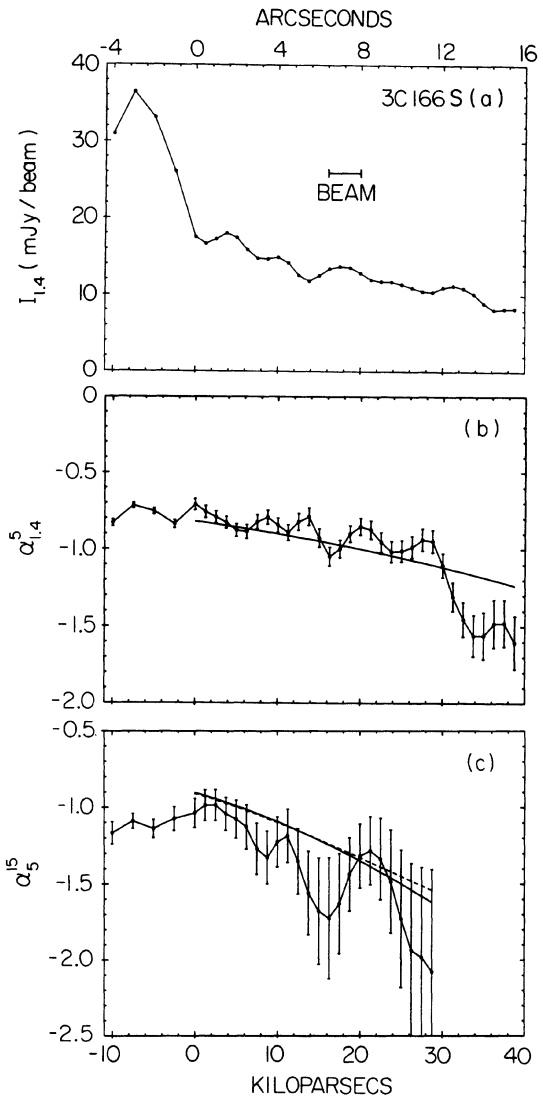

FIG.. 3. Map observables on a slice along the source axis for the southern lobe of 3C 166. The panels display 1.4 GHz total intensity (a), 1.4–5 GHz spectral index (b), and 5–15 GHz spectral index (c). The curves represent model fits discussed in the text.

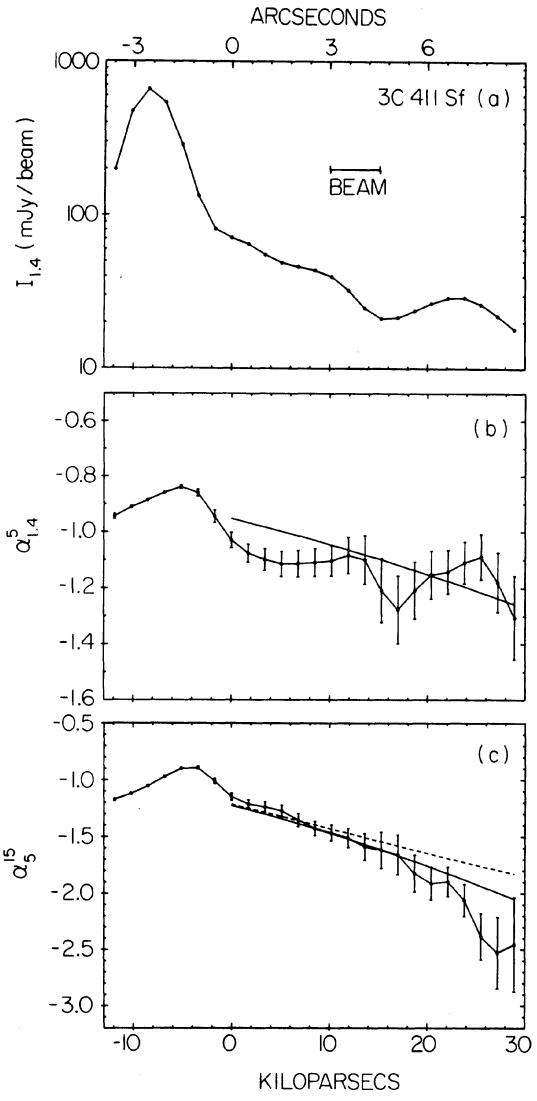

FIG. 4. Same as Fig. 3 except for the Sf lobe of 3C 411.

For the remainder of the lobe we can only say that the 15 GHz fractional polarization is less than about 50%.

The polarization position angle of the central component at 15 GHz is $61° \pm 2°$. When combined with values of $65° \pm 2°$ at 5 GHz and $100° \pm 5°$ at 1.4 GHz, we obtain a rotation measure of 15 ± 2 radian/m^2. As mentioned in Spangler and Bridle (1982), other portions of the source show very little difference in 1.4 and 5 GHz polarization position angles, indicating increased Faraday rotation in front of the central component. This could result either from small-scale changes in galactic Faraday rotation (Simonetti, Cordes, and Spangler 1984) or from a medium in the 3C 166 galaxy.

2) 3C 411

Polarized emission was detected at 15 GHz in the brighter portions of the source. The 15 GHz polarization position angles are plotted in Fig. 6, superposed on a contour map of the source. The length of each plotted vector is proportional to the fractional linear polarization at that point. Figure 6 shows that in this source the inferred magnetic field is also circumferential at the periphery of the lobe.

3C 411 is similar to 3C 166 in that the center of the Sf lobe is weakly polarized at 1.4 and 5 GHz, with strong depolarization, i.e., a reduction of 1.4 GHz fractional polarization relative to that at 5 GHz, indicating some form of Faraday depolarization. Again, attempts to distinguish mechanisms for reduction of linear polarization are compromised by the weakness of the polarized emission in the lobe interior at 15 GHz.

Where the signal-to-noise ratio is sufficiently high to permit a comparison, the 5 and 15 GHz emissions seem to be similarly polarized. In the Sf lobe along the source axis, the fractional polarization at 15 GHz is $\sim 10\%$, but appears to rise closer to the central component. The fractional polarization in the Np hot spot is $\sim 25\%$. Within our ability to measure, these are the same as at 5 GHz. This suggests that

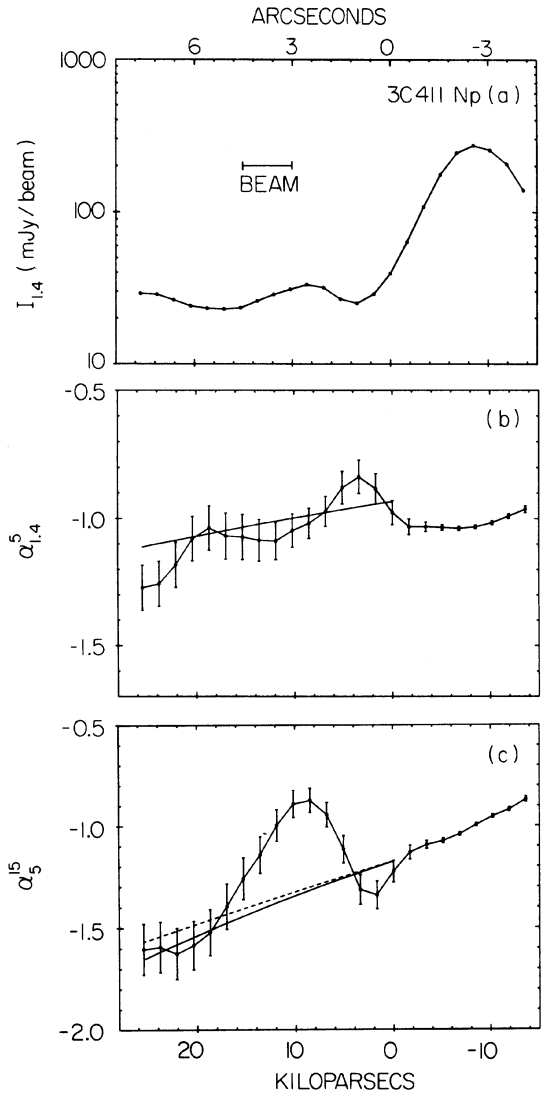

FIG. 5. Same as Fig. 3 except for the Np lobe of 3C 411.

Faraday effects are not important in the reduction of linear polarization at frequencies of 5 GHz and above.

IV. DISCUSSION

We have made a study of the 1.4–5 and 5–15 GHz spectral-index gradients across both lobes in the radio galaxy 3C 411, and the southern lobe in 3C 166. Our measurements have been compared with a model in which the radio emission is due to an isotropic ensemble of energetic electrons that are subject to synchrotron-radiation losses (synchrotron aging). If the age (time since acceleration) of the electrons at various locations in a lobe can be determined, we may infer a velocity between a parcel of lobe material and a hot spot.

The speed of advance of a hot spot relative to a parcel of lobe material is (Myers and Spangler 1985)

$$V_s = 30[(1+z)\nu_{\rm GHz}]^{1/2} B_{-5}^{3/2} [dX_0^{1/2}/dL_{\rm kpc}]^{-1} \text{ km/s}, \quad (1)$$

where $\nu_{\rm GHz}$ is the frequency of observation in GHz, B_{-5} is the magnetic field strength in units of 10^{-5} Gauss, z is the redshift of the source, and $[dX_0^{1/2}/dL_{\rm kpc}]^{-1}$ is a parameter proportional to the change in spectral index with distance (in kiloparsecs) from the hot spot. The parameter $X_0^{1/2}$ is defined in Myers and Spangler (1985) and is a dimensionless measure of the relative age of the radiating electrons. For $X_0^{1/2} \sim 0.5$, a substantial spectral-index change will be observed.

The above expressions are derived assuming the electrons retain the same pitch angles throughout their radiative lifetimes, and comprise the Kardashev (1962) and Pacholczyk (1970) (KP) model. If one assumes that the electron pitch angle is isotropized over periods that are short compared to the radiative lifetime of a particle, then the above equation should be multiplied by the time average of the pitch angle, i.e., $\langle \sin^2 \theta \rangle$, where the brackets stand for time average and θ is pitch angle. We have termed this model the Jaffe and Perola (1974) (JP) model. For a more thorough discussion of the differences between the two models, the reader is referred to Myers and Spangler (1985). As mentioned in that paper, differences between the models are not major.

Using the synchrotron-aging model of Myers and

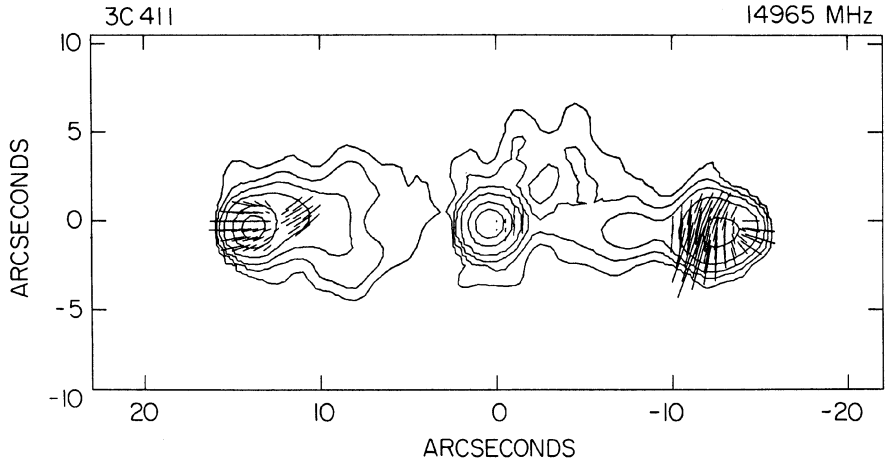

FIG. 6. Plot of electric field vectors at 14.965 GHz, superimposed on the total intensity map of Fig. 2(b). Contours are at 0.5, 1, 2, 5, 20, and 50% of the peak intensity.

TABLE I. Summary of separation speeds.

Source	Lobe	V_s (km/s)	V_s range (km/s)
	JP model		
3C 166	S	7 700	5 400–12 300
3C 411	Sf	13 600	10 900–19 400
3C 411	Np	16 300	10 600–32 400
	KP model		
3C 166	S	11 700	8 200–18 400
3C 411	Sf	20 100	15 700–29 000
3C 411	Np	24 700	16 000–49 500

Spangler (1985), we have obtained the best-fitting values for the lobe-hotspot separation speed. In all cases the model fits to the spectral-index data have been restricted to the lobe regions between the hot spots and central components. In this way we avoid regions of the sources where expansion losses may be important, e.g., in the hot spots. A discussion of corrections to the speed estimates not taken into account in the analysis presented here is given in Myers and Spangler (1985). We now discuss each source separately.

a) 3C 166

The best self-consistent model fits for the southern lobe, for a constant speed of separation, are shown by the curves in Fig. 3. The solid curve in Fig. 3(c) represents the predicted spectral index for the JP model, whereas the dashed curve represents that of the KP model. The speeds of separation of the hot spot and the lobe material are then 7700 and 11 700 km/s for the JP and KP models, respectively. We have used a value of 2.0×10^{-5} Gauss for the equipartition magnetic field in this lobe. These speed estimates are consistent with those reported in Myers and Spangler (1985) for the same lobe and are listed in Table I. Columns (1) and (2) indicate the source and lobe. The separation speeds consistent with the spectral-index data are listed in column (3), while column (4) lists their associated ranges. These ranges were empirically judged to delineate the limits of plausible fits to the data.

The data do not conform to a constant speed of separation through the entire lobe, as can be seen in Figs. 3(b) and 3(c). In the back of the lobe the spectral index is seen to steepen rapidly, possibly indicating that at some time in the past the speed of separation of the hot spot and the lobe material was substantially smaller. This does not introduce any difficulties if one postulates a high-density medium surrounding the central galaxy. The speed estimates for this region of the lobe are 2700 km/s (JP) and 3700 km/s (KP).

b) 3C 411

The curves in Fig. 4 represent the best self-consistent model fits for the Sf lobe. In Fig. 4(c) the solid and dashed curves represent the predicted 5–15 GHz spectral index (for a constant speed of separation) for the JP and KP models, respectively. The speed estimates for the Sf lobe are 13 600 km/s for the JP model and 20 100 km/s for the KP model.

These separation speeds are predicted on an adopted equipartition magnetic field of 2.5×10^{-5} Gauss, which is approximately half the value used by Myers and Spangler (1985) for their speed estimates. This difference results from our assumption in the present paper that the electron spectrum has a spectral index of 5/2, whereas the observationally inferred value of 3 was used by Myers and Spangler (1985). For electron spectral indices greater than 2, most of the energy resides in the lowest-energy electrons, so slight differences in the assumed spectral index can be important. The observed 1.4–5 GHz spectral index of ~ 1 is apparently the result of synchrotron losses, which do not affect the lowest-energy electrons. We therefore feel the present magnetic field value is a better estimate, but it is also clear that our analysis is uncomfortably sensitive to the assumption of equipartition.

From Eq. (1) we see that the speed of separation is proportional to the 3/2 power of the magnetic field so that our speed estimates for the Sf lobe are about a factor of 3 lower than previously reported. We also note that the previous speed estimates were calculated using only the 1.4–5GHz spectral-index gradient, whereas the present observations use both the 1.4–5 and 5–15 GHz data to better constrain the range of parameters used in the speed-estimate calculations.

The spectral-index model fits for a constant speed of separation are shown in Figs. 5(b) and 5(c) for the Np lobe. We have attempted to fit the parts of the slice not contaminated by the jet-like knot. The solid and dashed curves in Fig. 5(c) again represent the predicted 5–15 GHz spectral index for the JP and KP models, respectively. Using a value of 2.3×10^{-5} Gauss for the equipartition magnetic field in the Np lobe, we calculate a speed of separation of 16 300 km/s for the JP model. The speed of separation calculated using the KP model is 24 700 km/s.

The speed estimates for both the JP and KP models are listed in Table I. We note that these revised separation speeds are now quite consistent with the range found for other sources by Myers and Spangler (1985).

V. CONCLUSIONS

We have presented 15 GHz VLA observations of the double radio galaxies 3C 166 and 3C 411. These observations, together with previous 1.4 and 5 GHz VLA observations, have been used to study the frequency dependence of total intensity and polarization characteristics in these radio galaxies. Our conclusions are as follows:

(a) The new 15 GHz observations confirm the spectral steepening reported on the basis of earlier 1.4 and 5 GHz measurements, and have refined measurements of radiative lifetimes, presented as a relative speed of separation of the hot spots and lobe material. These separation speeds, 8000–12 000 km/s for the southern lobe of 3C 166 and 14 000–25 000 km/s for both lobes of 3C 411, are comparable to values obtained for other sources by Myers and Spangler (1985), Burch (1977, 1979), and Winter *et al.* (1980). These values are also in good agreement with hydrodynamical models of such sources (Norman *et al.* 1982), which interpret the measured speed as a combination of hot spot motion and backflow of beam material.

(b) In both 3C 166 and 3C 411 the 15 GHz fractional linear polarization is comparable to that at 5 GHz and much larger than at 1.4 GHz. These results indicate geometric depolarization for frequencies of 5 GHz and above for both sources.

This work was supported by NSF Grant No. AST 82-17714.

REFERENCES

Bridle, A. H. (1982). In *Extragalactic Radio Sources*, edited by D. S. Heeschen and C. M. Wade (Reidel, Dordrecht).
Burch, S. F. (1977). Mon. Not. R. Astron. Soc. **180**, 623.
Burch, S. F. (1979). Mon. Not. R. Astron. Soc. **186**, 519.
Jaffe, W. J., and Perola, G. C. (1974). Astron. Astrophys. **26**, 423.
Kardashev, N. S. (1962). Soviet Astron.—AJ **6**, 317.
Myers, S. T., and Spangler, S. R. (1985). Astrophys. J. **291**, 52.
Norman, M. L., Smarr, L., Winkler, H. A., and Smith, M. D. (1982). Astron. Astrophys. **113**, 285.
Pacholczyk, A. G. (1970). *Radio Astrophysics* (Freeman, San Francisco).
Simonetti, J. H., Cordes, J. M., and Spangler, S. R. (1984). Astrophys. J. **284**, 126.
Spangler, S. R., and Bridle, A. H. (1982). Astron. J. **87**, 1270.
Spangler, S. R., and Pogge, J. J. (1984). Astron. J. **89**, 342.
Winter, A., *et al.* (1980). Mon. Not. R. Astron. Soc. **192**, 931.